









Structural 130 K phase transition and emergence of a two-ion Kondo state in $\text{Ce}_2\text{Rh}_2\text{Ga}$ explored by $^{69,71}\text{Ga}$ nuclear quadrupole resonance

Sh. Yamamoto ^{1,2,*}, T. Fujii,² S. Luther,^{1,3} H. Yasuoka ², H. Sakai ⁴, F. Bärtl ^{1,3}, K. M. Ranjith ², H. Rosner,² J. Wosnitza,^{1,3} A. M. Strydom ^{2,5}, H. Kühne ¹ and M. Baenitz ²


¹Hochfeld-Magnetlabor Dresden (HLD-EMFL) and Würzburg-Dresden Cluster of Excellence *ct.qmat*, Helmholtz-Zentrum Dresden-Rossendorf, 01328 Dresden, Germany

²Max Planck Institute for Chemical Physics of Solids, D-01187 Dresden, Germany

³Institut für Festkörper- und Materialphysik, TU Dresden, 01062 Dresden, Germany

⁴Advanced Science Research Center, Japan Atomic Energy Agency, Tokai, Ibaraki 319-1195, Japan

⁵Highly Correlated Matter Research Group, Physics Department, University of Johannesburg, P.O. Box 524, Auckland Park 2006, South Africa

 (Received 13 May 2022; revised 26 August 2022; accepted 26 August 2022; published 14 September 2022)

We have studied the microscopic magnetic properties, the nature of the 130 K phase transition, and the ground state in the recently synthesized compound $\text{Ce}_2\text{Rh}_2\text{Ga}$ by use of $^{69,71}\text{Ga}$ nuclear quadrupole resonance (NQR). The NQR spectra clearly show an unusual phase transition at $T_i \sim 130$ K, yielding a splitting of the high-temperature single NQR line into two well-resolved NQR lines, providing evidence for two crystallographically inequivalent Ga sites. The NQR frequencies are in good agreement with fully relativistic calculations of the band structure. Our NQR results indicate the absence of magnetic or charge order down to 0.3 K. The temperature dependence of the spin-lattice relaxation rate $1/T_1$ shows three distinct regimes, with onset temperatures at T_i and 2 K. The temperature-independent $1/T_1$, observed between T_i and 2 K, crosses over to a Korringa process, $1/T_1 \propto T$, below ~ 2 K, which evidences a rare two-ion Kondo scenario: The system evolves into a dense Kondo coherent state below 2.0 and 0.8 K probed by the two different Ga sites.

DOI: [10.1103/PhysRevB.106.115125](https://doi.org/10.1103/PhysRevB.106.115125)

I. INTRODUCTION

Among the correlated $4f$ -ion systems, there are only a few compounds in which a structural instability at high temperatures has an effect on the ground state and especially on the correlations among the $4f$ ions and conduction electrons. While in Yb systems charge ordering or even significant intermediate-valence behavior can occur, Ce systems are usually characterized by a rather stable valence [1,2]. $\text{Ce}_2\text{Rh}_2\text{Ga}$ seems to be an exception to the rule. This material is dimorphic, with high- (HT) and low-temperature (LT) forms, yielding an orthorhombic La_2Ni_3 -type (space group $Cmce$) and monoclinic (space group $C2/c$) structure at room temperature, respectively, depending on thermal treatments during the sample synthesis [3].

In the so-called HT- $\text{Ce}_2\text{Rh}_2\text{Ga}$ form, a structural phase transition at 130 K changes the ground state due to a reconstruction of the Fermi surface and a slight increase of the Ce valence beyond $3+$ [3–5]. The question arises how this influences the coupling of charge and spin. As a consequence of the 130 K phase transition, the coupling between

the cerium ions is reduced [6], which is a prerequisite for the formation of the heavy-fermion state. Furthermore, the low-temperature phase exhibits two inequivalent Ce ions, which are exposed to Kondo screening at different temperatures. Multi-ion Kondo physics is rare and only poorly explored. Exceptions are theoretical studies [7–9] as well as experimental studies of site-dependent magnetic transitions for $\text{Ce}_3\text{Pd}_{20}\text{Si}_6$ [10], $\text{Ce}_3\text{PtIn}_{11}$ [11–13], and Ce_7Ni_3 [14]. Here, site-selective microscopic experiments can provide crucial information for understanding the underlying physics.

In this paper, we study the HT form, HT- $\text{Ce}_2\text{Rh}_2\text{Ga}$, which exhibits a unique phase transition at $T_i \sim 130$ K that is accompanied by signatures in the specific heat and magnetic susceptibility. Taking these anomalies into account, the authors in Ref. [3] argued that below T_i , HT- $\text{Ce}_2\text{Rh}_2\text{Ga}$ undergoes an antiferromagnetic (AFM) order. Alternatively, a charge density wave (CDW) scenario is also possible. However, the origin of the 130 K phase transition is not yet fully understood.

The structural phase change across T_i has been studied by x-ray diffraction experiments [4]. The structure changes from a room-temperature orthorhombic phase ($a = 5.845$ Å, $b = 9.573$ Å, $c = 7.496$ Å) to a monoclinic phase with non-merohedral twinning of the space group $C2/m$ ($a = 9.401$ Å, $b = 5.807$ Å, $c = 7.595$ Å, $\beta = 91.89^\circ$). In the monoclinic phase below T_i , two inequivalent Ga sites are expected [4,6]. Recent resonant x-ray emission spectroscopy experiments indicate that the average Ce valence v increases by $\sim 0.7\%$ from the orthorhombic ($v \sim 3.053$) to the monoclinic ($v \sim 3.075$)

*s.yamamoto@hzdr.de

phase [5]. In addition, our specific-heat data indicate the occurrence of a heavy-fermion state [6].

The aim of this paper is to provide microscopic information on the nature of the 130 K phase transition, as well as on the formation of the correlated ground state. The present NQR results clearly show that neither an AFM nor CDW scenario can be considered. The symmetry reduction below 130 K yields two magnetically inequivalent Ce and Ga sites in the lattice. The NQR spin-lattice relaxation measured at these two Ga sites clearly indicates the formation of a heavy-fermion state, but the transition to this occurs at two distinct temperatures. Thus, in $\text{Ce}_2\text{Rh}_2\text{Ga}$ there exist two cerium ions which are differently shielded by the surrounding conduction electrons (two-ion Kondo effect). The two cerium sublattices are magnetically coupled to each other. $\text{HT-Ce}_2\text{Rh}_2\text{Ga}$ is thus a rather unusual $4f$ system which can serve as a platform to study the two-ion Kondo physics.

II. EXPERIMENT

In this study, we focused on the Ga NQR in $\text{HT-Ce}_2\text{Rh}_2\text{Ga}$, where each Ce atom is surrounded by four Ga neighbors, forming edge-sharing CeGa_4 tetrahedra [6]. The sample was prepared in the same way as described in Ref. [3], i.e., the arc-melted ingot was annealed at 900 °C for 30 days in an evacuated quartz tube and then quenched in cold water. The annealed ingot was checked by x-ray diffraction to ensure the $\text{HT-Ce}_2\text{Rh}_2\text{Ga}$ existence of the phase, and then powdered to about 200 μm particle size. The powdered sample was mixed with paraffin so that the skin-depth effect due to eddy currents by radio-frequency excitation during the NQR measurements is negligible [6].

The Ga nuclei have two stable isotopes, ^{69}Ga and ^{71}Ga . Both of them have a nuclear spin of $I = 3/2$, and the nuclear gyromagnetic ratio γ , the nuclear quadrupole moment Q , and the natural abundance A are $^{69}\gamma = 10.2192 \text{ MHz/T}$, $^{69}Q = 0.178 \text{ b}$, $^{69}A = 60\%$ for ^{69}Ga , and $^{71}\gamma = 12.9847 \text{ MHz/T}$, $^{71}Q = 0.112 \text{ b}$, $^{71}A = 40\%$ for ^{71}Ga , respectively. The ratios of γ and Q between the two isotopes are $(^{69}\gamma/^{71}\gamma) = 0.7870$ and $(^{69}Q/^{71}Q) = 1.589$. The NQR spectra and the nuclear relaxation times were measured using a standard pulsed (spin-echo) NMR apparatus (TecMag-Apollo). The NQR spectra were recorded by the frequency-sweep method. Further experimental details are described in note 2 of the Supplemental Material [6].

III. Ga NQR SPECTRA

For searching the NQR signal, we consider the nuclear energy levels E_m obtained from the nuclear quadrupole Hamiltonian, which can be expressed in the case of a nonaxial field gradient for $I = 3/2$ as [15]

$$E_{\pm 3/2} = \frac{1}{2}h\nu_Q\sqrt{1 + \frac{\eta^2}{3}}, \quad (1)$$

$$E_{\pm 1/2} = -\frac{1}{2}h\nu_Q\sqrt{1 + \frac{\eta^2}{3}}, \quad (2)$$

$$\nu_Q \equiv \frac{3e^2qQ}{\hbar 2I(2I - 1)}, \quad (3)$$

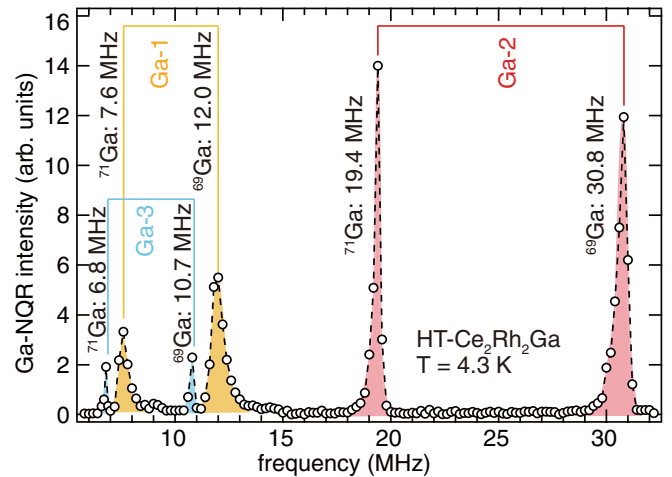


FIG. 1. Ga-NQR spectra of $\text{HT-Ce}_2\text{Rh}_2\text{Ga}$ at 4.3 K. There are three pairs of ^{69}Ga and ^{71}Ga NQR signals, Ga-1, 2, and 3, that are assigned to three inequivalent Ga sites.

where ν_Q denotes the quadrupole coupling between the electric-field gradient (EFG) stemming from an asymmetric charge distribution at the nuclear site q and the nuclear quadrupole moment Q . The NQR occurs for the transition between two levels $\pm 1/2$ and $\pm 3/2$, and the NQR frequency can be written as $\nu_{\text{NQR}} = \nu_Q\sqrt{1 + \eta^2/3}$ for $I = 3/2$. Hence, only one NQR line for $I = 3/2$, ^{69}Ga and ^{71}Ga , is expected.

In Fig. 1, we show a broadband Ga NQR spectrum at 4.3 K (in the monoclinic phase). We observe three pairs of ^{69}Ga and ^{71}Ga signals labeled Ga-1, Ga-2, and Ga-3. The observed frequency ratios for the NQR pairs ^{69}Ga and ^{71}Ga NQR are 1.572 ± 0.005 , 1.589 ± 0.002 , and 1.588 ± 0.010 , respectively. These numbers agree very well with the ratio of $^{69}Q/^{71}Q = 1.589$, confirming the validity of the spectral assignment.

Focusing on the ^{69}Ga NQR signal, we show the temperature dependence of the NQR spectrum in Fig. 2(a), including data above T_t (in the orthorhombic phase). The single Ga-NQR signal, $^{69}\text{Ga-0}$, shows spectral broadening with decreasing temperature from 300 to 170 K, presumably due to some inhomogeneous distribution of the phase transition. Below ~ 130 K, the single peak Ga-0 splits into two lines, Ga-1 and Ga-2. We observe an additional Ga-NQR line, $^{69}\text{Ga-3}$, at 10.8 MHz. Since the $^{69}\text{Ga-3}$ signal yields a constant temperature dependence, we associate this with a signal either from twin boundaries or an impurity phase. The Ga-1 (Ga-2) peak shifts to lower (higher) frequency with decreasing temperature, reaching 12 MHz (30.8 MHz) at 4.3 K [see Fig. 2(b)].

A question arises concerning the origin of the line splitting below T_t , because the first report of $\text{Ce}_2\text{Rh}_2\text{Ga}$ proposed an AFM order below T_t [3]. However, if this would be the case, we would see an NQR line splitting due to the local hyperfine field from ordered Ce moments. As clearly seen in Fig. 2, we observe very sharp NQR lines for each Ga-1 and Ga-2 site at low temperatures, definitively affirming the absence of AFM order. Further, as shown in the following, the temperature dependence of the spin-lattice relaxation

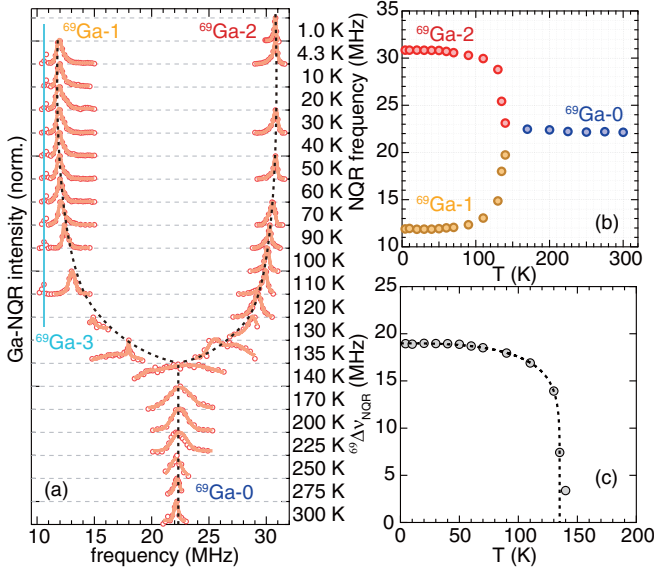


FIG. 2. (a) Temperature dependence of the ^{69}Ga -NQR spectra of HT- $\text{Ce}_2\text{Rh}_2\text{Ga}$. ^{69}Ga -0 is associated with the single Ga site in the orthorhombic phase ($T > T_i$), and the ^{69}Ga -1 and ^{69}Ga -2 signals stem from two inequivalent Ga sites in the monoclinic phase ($T < T_i$). (b) Temperature dependence of the ^{69}Ga -NQR peak frequencies extracted by using a Gaussian fit. Blue circles are data from ^{69}Ga -0 above T_i . Yellow and red circles are data from ^{69}Ga -1 and ^{69}Ga -2, respectively. (c) Temperature dependence of $^{69}\Delta\nu_{\text{NQR}} = \nu_{\text{NQR}}(\text{Ga-2}) - \nu_{\text{NQR}}(\text{Ga-1})$. The dashed line is a guide to the eye.

rate does not display any peaks related to magnetic order [Fig. 3(a)], which excludes a possible scenario in which local fields from the Ce ions cancel each other at the Ga site. Preliminary muon spin relaxation (μSR) measurements also support the absence of magnetic order above 2 K [16]. Furthermore, any charge and/or spin density wave order is excluded. In these cases, we should see a characteristic inhomogeneous line broadening due to the EFG or internal field modulation.

In order to check the site assignment above we performed EFG calculations based on the band structure calculated using the density functional theory solid-state code FPLO [17]. The k meshes in both structures were carefully converged with respect to the total energy and the calculated EFG. We used the Perdew-Wang parametrization of the local density approximation for the exchange-correlation functional [18]. To account for the strong electronic correlations of the Ce $4f$ electrons, we applied the local density approximation (LDA+ U) approach with $U = 6$ eV for the Ce $4f$ states. Varying U by ± 1 eV did not show significant changes. Alternatively, treating the Ce $4f$ electron as a core state in the frozen core approximation yields very similar results for the EFG's on the Ga sites. The quadrupole coupling ν_Q can be obtained by calculating the EFG at each Ga nuclear site which is defined as the second partial derivative of the electrostatic potential at the position of the nucleus. We summarized the obtained maximum EFG, V_{ZZ} , asymmetry parameter [$\eta = (V_{XX} - V_{YY})/V_{ZZ}$], and the quadrupole-coupling constant ν_Q in Table I. We compare then the extracted NQR frequencies with the experimental values. The NQR frequencies obtained

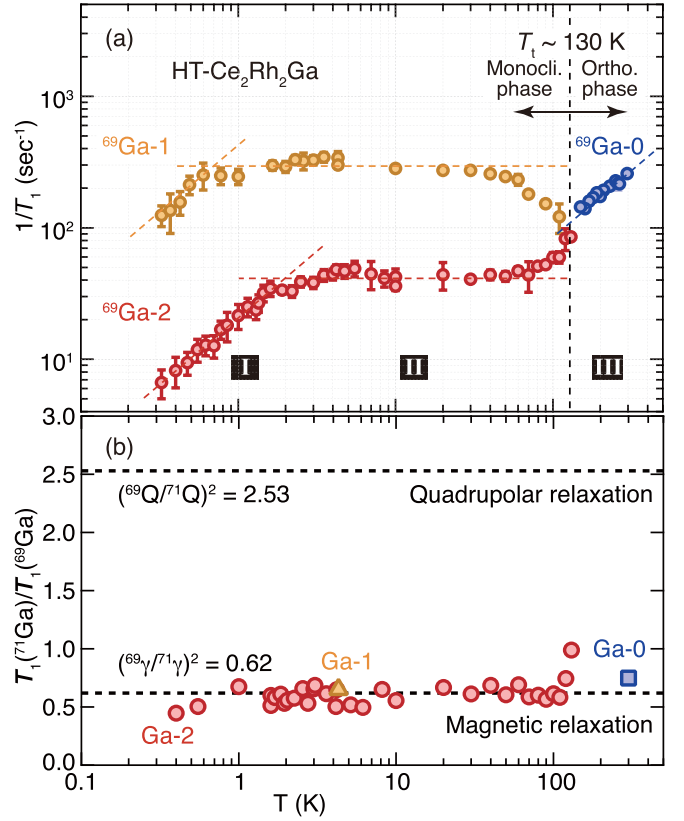


FIG. 3. (a) Temperature dependence of the ^{69}Ga -NQR spin-lattice relaxation rate $1/T_1$ for the ^{69}Ga -0 (blue), ^{69}Ga -1 (yellow), and ^{69}Ga -2 (red) lines. There are three distinct temperature regions where the relaxation processes yield a different characteristic behavior. Region III is in the orthorhombic phase above $T_i \sim 130$ K and $1/T_1$ behaves as for a Korringa process. Regions I and II lie within the monoclinic phase below T_i . (b) The ratios of T_1 for the two Ga isotopes, $^{71}\text{Ga}/^{69}\text{Ga}$, for the Ga-0, Ga-1, and Ga-2 lines are shown by blue, yellow, and red symbols, respectively.

from our experiments are in good agreement with the calculated values, assuring that the site assignment is correct. The maximum principal axis V_{ZZ} of the calculated EFG points along the b axis of the monoclinic structure for both the Ga-1 and Ga-2 sites.

Our specific-heat and susceptibility results signal a first-order transition in a narrow temperature region around T_i [3,6]. On the other hand, a gradual variation of the NQR frequency has been observed from T_i down to ~ 80 K. Below T_i , the variation of the NQR frequencies couples predominantly to the evolving structural monoclinicity. The temperature-dependent splitting of the NQR spectra can be evaluated as $^{69}\Delta\nu_{\text{NQR}} = \nu_{\text{NQR}}(\text{Ga-2}) - \nu_{\text{NQR}}(\text{Ga-1})$, and is depicted in Fig. 2(c). The lattice parameters [3] and Ce $4f$ valence [5] also display a continuous variation with respect to temperature similar to that of the NQR frequency below T_i .

IV. NUCLEAR MAGNETIC RELAXATION

The nuclear spin-lattice relaxation time T_1 has been measured by the inversion-recovery method, where the recovery

TABLE I. Calculated EFG tensors and quadrupole coupling constants in HT-Ce₂Rh₂Ga (see main text). Ga-0 is associated with the Ga site in the orthorhombic phase above T_i . Ga-1 and Ga-2 are two inequivalent Ga sites in the monoclinic phase below T_i , respectively. The Wyckoff position for each Ga site is also listed.

Ga sites	Calculation				Experiment
	$V_{ZZ} = \partial V / \partial x_Z \partial x_Z$ (10^{21} V/m ²)	η	ν_Q (MHz)	ν_{NQR} (MHz)	ν_{NQR} (MHz)
Ga-0 (<i>Cmce</i> , 4a)	10.199	0.79	21.9	24.1	22.336
Ga-1 (<i>C2/m</i> , 2a)	-6.609	0.85	14.2	15.8	11.964
Ga-2 (<i>C2/m</i> , 2d)	13.197	0.65	28.4	30.3	30.758

of the nuclear magnetization $M(t)$, measured by the spin-echo amplitude after the application of an inversion pulse, recovers as a single-exponential function for $I = 3/2$, and was fitted by the following function,

$$M(t) = M_0 \{1 - c_0 \exp[-(3t/T_1)^\beta]\}, \quad (4)$$

where M_0 , c_0 , t , and β are the equilibrium nuclear magnetization, inversion factor ($c_0 = 2$ for complete inversion), the time after the inversion pulse, and the stretching exponent [6], respectively. We show the temperature dependences of $1/T_1$ for the ⁶⁹Ga-0, ⁶⁹Ga-1, and ⁶⁹Ga-2 lines in Fig. 3(a). There are three distinct temperature regions where the relaxation processes have different characteristic features: Regions I and II below T_i are in the monoclinic phase, while region III above T_i is in the orthorhombic phase. Before discussing the mechanism in each region, we have to clarify if the origin of the relaxation mechanism is magnetic or quadrupolar. The ratio of T_1 for the two isotopes, ⁷¹Ga and ⁶⁹Ga, is plotted in Fig. 3(b). As can be seen in the figure, the ratio is ~ 0.62 for all temperatures, which is just equal to $(^{69}\gamma/^{71}\gamma)^2$, assuring that the relaxation process is governed by magnetic fluctuations, and not by fluctuations of the EFG (a quadrupolar relaxation process would give a ratio of 2.5). In the present case of a purely magnetic relaxation process, the relaxation rate $1/T_1$ is generally expressed as [19]

$$\frac{1}{T_1} = \frac{k_B T}{(\gamma_e \hbar)^2} 2(\gamma_N A_\perp)^2 \sum_q f^2(\mathbf{q}) \frac{\text{Im} \chi_\perp(\mathbf{q}, \omega_0)}{\omega_0}, \quad (5)$$

where γ_e , $\text{Im} \chi_\perp(\mathbf{q}, \omega_0)$, and ω_0 are the electronic gyromagnetic ratio, the perpendicular component of the imaginary part of the dynamical susceptibility $\chi(\mathbf{q}, \omega_0)$, with respect to the quantization axis, and the nuclear Larmor frequency, respectively. $f(\mathbf{q})$ is the hyperfine form factor.

For $4f$ metals such as Ce₂Rh₂Ga, we have two relaxation channels: one from electron-hole pair excitations across the Fermi level and the other is due to exchange-coupled Ce local spin fluctuations. For the former case, $\chi(\mathbf{q}, \omega_0)$ is temperature independent and $f(\mathbf{q}) = 1$, hence, $1/T_1 \propto T$ (Korringa process) [20], while in the latter case, $\chi(\mathbf{q}, \omega_0)$ may yield a strong \mathbf{q} and temperature dependence, depending on ferro- or antiferromagnetic correlations. In such a case, we have a temperature-independent relaxation process, $1/T_1 \propto A^2 J(J+1)/3\omega_{\text{ex}}$, where $J\mu_B$ is the Ce localized moment and ω_{ex} is the exchange frequency, which is estimated from the Weiss constant of the Curie-Weiss (CW) susceptibility [21,22]. Since the bulk susceptibility of HT-Ce₂Rh₂Ga shows a CW temperature dependence with a Weiss constant $\theta_p \sim -140$ K in the

orthorhombic phase [3,6], the primary relaxation process is considered to stem from AFM spin fluctuations.

$F(\mathbf{q})$, the \mathbf{q} -summed $f^2(\mathbf{q})$, should be calculated from the local geometrical factor at the Ga site [6]. We start to discuss region III, where we see the Korringa behavior $1/T_1 \propto T$. This is not compatible with the localized picture of exchange-coupled $4f$ Ce³⁺ moments. We calculate that the hyperfine form factor $F(\pi, \pi, \pi)$ is approximately $1/64$ of $F(0, 0, 0)$, by assuming an isotropic hyperfine coupling constant between the Ga and Ce ions in the orthorhombic phase, taking into account the Ce ions up to the third nearest neighbor of the Ga ion [6]. Correspondingly, the contribution of AFM fluctuations to $1/T_1$ is strongly suppressed due to the form factor in region III, and the Korringa process exceeds the contribution by AFM fluctuations, which results in the observed linear temperature dependence of $1/T_1$.

Because of the lowering of the local symmetry at the Ga sites below T_i (monoclinic phase), one can expect that the AFM fluctuations are not screened in region II, which results in the temperature-independent relaxation process via fluctuations of the local Ce moment contributions at the Ga-1 and Ga-2 sites. In region I, $1/T_1$ exhibits again a Korringa behavior below 0.8 K for Ga-1 and below 2.0 K for Ga-2. For the Ga-2 site, we also confirmed the onset of Kondo screening at 2 K by measurements of the T_1 relaxation rate of the second isotope ⁷¹Ga [see Fig. S2(c) in the Supplemental Material [6]]. This crossover of the relaxation process firmly indicates that the Ce $4f$ state is strongly hybridized with the conduction electrons, forming a coherent heavy-electron state, i.e., a dense Kondo coherent state. This formation of a Kondo coherent state has also been reported from measurements of temperature-dependent $1/T_1$ for other Ce-based heavy fermions [23]. It is worth pointing out that the coherence temperature is different for Ga-1 (~ 0.8 K) and Ga-2 (~ 2.0 K). This presumably results from different Kondo screening, i.e., different Kondo temperatures for the two inequivalent Ce ions. The evolution of the local Kondo shielding as a function of temperature is probed at the two different Ga sites by the relaxation rate $1/T_1$. The Kondo shielding results from a complex interplay between the Kondo and Ruderman-Kittel-Kasuya-Yosida (RKKY) interactions. The resulting field of the ‘‘Kondo cloud’’ is then transferred to the Ga ions (via conduction-electron polarization). Our band-structure calculations show that two bands cross the Fermi energy in the monoclinic phase. In this respect, HT-Ce₂Rh₂Ga is a multi-band system below 130 K. Specific-heat results obtained on HT-Ce₂Rh₂Ga polycrystals also indicate the formation of a heavy-fermion state with a Sommerfeld coefficient $\gamma = 1$ J/mol_{f.u.} K² below 2 K [6].

V. CONCLUSION

We investigated the microscopic nature of the 130 K phase transition and the formation of the unusual ground state of HT-Ce₂Rh₂Ga using NQR. The spectral variation with temperature across $T_l \sim 130$ K provides evidence for the absence of magnetic or charge order. The temperature dependence of $1/T_1$ is governed by the antiferromagnetically coupled Ce $4f$ local spin fluctuations, but both above T_l , and below 0.8 K for the Ga-1 site and below 2.0 K for the Ga-2 site, $1/T_1(T)$ behaves Korringa-like. Here, we argue that the former is due to the screening of the AFM fluctuations by the hyperfine form factor, and the latter is due to the formation of a Kondo coherent state. Particularly, the emergence of a two-ion Kondo state with inequivalent Ce ions being screened at different temperatures is the most important outcome of the present study. It can be assumed that the Fermi surface is very anisotropic in Ce₂Rh₂Ga, which makes future studies of single crystals very interesting. A spatially anisotropic conductivity limits

the RKKY interaction in real space, and thus affects the competition with the isotropic Kondo interaction. This creates an anisotropic Kondo system with multi-ion Kondo physics, which is certainly an exciting topic for future studies.

ACKNOWLEDGMENTS

We thank A. Tursina for fruitful discussions and for leading our understanding of the crystal structure of the title compound. U. Nitzsche is acknowledged for technical support. We acknowledge the support of the HLD at HZDR, member of the European Magnetic Field Laboratory (EMFL), the Deutsche Forschungsgemeinschaft (DFG) through SFB 1143, and the Würzburg-Dresden Cluster of Excellence on Complexity and Topology in Quantum Matter–*ct.qmat* (EXC 2147, Project ID 390858490). A.M.S. thanks the South Africa National Research Foundation (93549) and the URC/FRC of UJ for financial assistance.

- [1] N. B. Brandt and V. V. Moshchalkov, Concentrated Kondo systems, *Adv. Phys.* **33**, 373 (1984).
- [2] A. C. Hewson, D. M. Newns, J. W. Rasul, N. Read, H. U. Desgranges, and P. Strange, Models for intermediate valence systems and Kondo lattices - Applications to cerium and ytterbium compounds, in *Theory of Heavy Fermions and Valence Fluctuations*, edited by T. Kasuya and T. Sato, Springer Series in Solid State Sciences Vol. 62 (Springer, Berlin, 1985).
- [3] S. Nesterenko, A. Tursina, M. Pasturel, S. Xhakaza, and A. Strydom, Two polymorphs of a new intermetallic Ce₂Rh₂Ga – crystal structure and physical properties, *J. Alloys Compd.* **844**, 155570 (2020).
- [4] A. Dudka, S. Nesterenko, and A. Tursina, Multi-temperature x-ray diffraction study of a reversible structural phase transition in the high-temperature polymorph of Ce₂Rh₂Ga compound, *J. Alloys Compd.* **890**, 161759 (2022).
- [5] H. Sato, T. Matsumoto, N. Kawamura, K. Maeda, T. Takabatake, and A. M. Strydom, Valence transition of the intermetallic compound Ce₂Rh₂Ga probed by resonant x-ray emission spectroscopy, *Phys. Rev. B* **105**, 035113 (2022).
- [6] See Supplemental Material at <http://link.aps.org/supplemental/10.1103/PhysRevB.106.115125> for the crystal structures of HT-Ce₂Rh₂Ga, experimental details of the NQR measurements, the calculation of $F(\mathbf{q})$, and macroscopic data, which includes Refs. [3–5].
- [7] P. A. Lee, T. M. Rice, J. W. Serene, L. J. Sham, and J. W. Wilkins, Theories of heavy-electron systems, *Comments Condens. Matter Phys.* **12**, 99 (1986).
- [8] A. Benlagra, L. Fritz, and M. Vojta, Kondo lattices with inequivalent local moments: Competitive versus cooperative Kondo screening, *Phys. Rev. B* **84**, 075126 (2011).
- [9] M. Jiang, Enhanced antiferromagnetic ordering tendency in the staggered periodic Anderson model, *Phys. Rev. B* **101**, 235124 (2020).
- [10] S. Paschen, M. Müller, J. Custers, M. Kriegisch, A. Prokofiev, G. Hilscher, W. Steiner, A. Pikul, F. Steglich, and A. M. Strydom, Quantum critical behaviour in Ce₃Pd₂₀Si₆?, *J. Magn. Magn. Mater.* **316**, 90 (2007).
- [11] J. Prokleška, M. Kratochvílová, K. Uhlířová, V. Sechovsky, and J. Custers, Magnetism, superconductivity, and quantum criticality in the multisite cerium heavy-fermion compound Ce₃PtIn₁₁, *Phys. Rev. B* **92**, 161114(R) (2015).
- [12] S. Kambe, H. Sakai, Y. Tokunaga, R. E. Walstedt, M. Kratochvílová, K. Uhlířová, and J. Custers, ¹¹⁵In NQR study with evidence for two magnetic quantum critical points in dual Ce site superconductor Ce₃PtIn₁₁, *Phys. Rev. B* **101**, 081103(R) (2020).
- [13] H. Fukazawa, K. Kumeda, N. Shioda, Y. Lee, Y. Kohori, K. Sugimoto, D. Das, J. Bławat, and D. Kaczorowski, Successive magnetic transitions in the heavy-fermion superconductor Ce₃PtIn₁₁ studied by ¹¹⁵In nuclear quadrupole resonance, *Phys. Rev. B* **102**, 165124 (2020).
- [14] K. Umeo, Y. Echizen, M. H. Jung, T. Takabatake, T. Sakakibara, T. Terashima, C. Terakura, C. Pfleiderer, M. Uhlarz, and H. v. Löhneysen, Field-induced magnetic transition in the heavy-fermion antiferromagnet Ce₇Ni₃, *Phys. Rev. B* **67**, 144408 (2003).
- [15] T. P. Das and E. L. Hahn, *Nuclear Quadrupole Resonance Spectroscopy* (Academic Press, New York, 1958).
- [16] A. M. Strydom, ISIS μ SR Experimental Report No. 2010475 (private communication).
- [17] K. Koepnick and H. Eschrig, Full-potential nonorthogonal local-orbital minimum-basis band-structure scheme, *Phys. Rev. B* **59**, 1743 (1999).
- [18] J. P. Perdew and Y. Wang, Accurate and simple analytic representation of the electron-gas correlation energy, *Phys. Rev. B* **45**, 13244 (1992).
- [19] T. Moriya, The effect of electron-electron interaction on the nuclear spin relaxation in metals, *J. Phys. Soc. Jpn.* **18**, 516 (1963).
- [20] J. Korringa, Nuclear magnetic relaxation and resonance line shift in metals, *Physica* **16**, 601 (1950).
- [21] T. Moriya, Nuclear magnetic relaxation in antiferromagnetics, *Prog. Theor. Phys.* **16**, 23 (1956).
- [22] T. Moriya, Nuclear magnetic relaxation in antiferromagnetics, II, *Prog. Theor. Phys.* **16**, 641 (1956).
- [23] Y. Kawasaki, K. Ishida, Y. Kitaoka, and K. Asayama, K. Si-NMR study of antiferromagnetic heavy-fermion compounds CePd₂Si₂ and CeRh₂Si₂, *Phys. Rev. B* **58**, 8634 (1998).